https://doi.org/10.5194/egusphere-2025-4594
Preprint. Discussion started: 2 October 2025

Storm-Time Asymmetries at Magnetic Conjugate Points: A Distribution-Aware Benchmark for GNSS

Serhat Korlaelci[1], Ramazan Atici[1], Selcuk Sagir[1]

[1] Department of Physics, Faculty of Arts and Sciences, Muş Alparslan University, 49250 Muş, Türkiye

Correspondence: Serhat Korlaelci (s.korlaelci@alparslan.edu.tr)

Abstract

Geomagnetic storms disrupt the Global Navigation Satellite System (GNSS) and transionospheric links through rapid asymmetric ionospheric variability. In this study, three widely used empirical models (IRI-2016, IRI-Plas, and NeQuick2) were used against GNSS-derived Total Electron Content (TEC) at two magnetic conjugate pairs (mid- and low-latitude) during the geomagnetic storm of August 25–27, 2018. Rather than assessing storm-time predictability, these models were employed as quiet-time reference baselines to quantify storm-time deviations and hemispheric asymmetry. Model performance was evaluated using the Mean Absolute Error (MAE), Root Mean Square Error (RMSE), and distribution-aware Kullback–Leibler divergence (KLD). This study introduces a novel conjugate-point validation framework augmented by KLD that uniquely captures both magnitude errors and structural distributional mismatches between hemispheres. This is a critical aspect of GNSS reliability that is overlooked by conventional metrics. The results indicate a phase-dependent performance: all models exhibit degradation during the main phase, with the largest errors and structural mismatches occurring at the equator. KLD reveals distributional distortions (variance, skewness, tails) that MAE and RMSE cannot, particularly at the storm onset. NeQuick2 demonstrates superior performance only during the recovery phase, which is consistent with its solar-flux-driven parameterization but limited topside representation. By integrating a conjugate-point framework with distribution-aware validation, this study elucidates where empirical baselines fail under storm conditions, and why hemispheric responses diverge. This approach clarifies the model limitations relevant to GNSS reliability and motivates the development of hybrid data-assimilative schemes that incorporate dynamic drivers while being evaluated with both magnitude- and structure-sensitive metrics.

Keywords. Total Electron Content (TEC); GNSS; IRI-2016; NeQuick2; Conjugate Points; Kullback-Leibler Divergence (KLD)

https://doi.org/10.5194/egusphere-2025-4594
Preprint. Discussion started: 2 October 2025

Short Summary

Ionospheric storms affect GNSS differently in conjugate hemispheres. Using GNSS-derived TEC during the 25–27 Aug 2018 storm, we assess IRI-2016, IRI-Plas, and NeQuick2 as quiet-time baselines. Magnitude errors (MAE, RMSE) and structure-sensitive KLD show phase-dependent degradation, with equatorial asymmetries strongest. This framework reveals hidden mismatches overlooked by conventional metrics and improves GNSS reliability assessment.

1 Introduction

The ionospheric response to geomagnetic storms remains a significant challenge in space weather and wireless communication research because of its nonlinear dynamics (Bojilova et al., 2024) and substantial impact on Global Navigation Satellite System (GNSS) positioning, including scintillation-induced degradation (Aguiar et al., 2025; Yang et al., 2020), satellite links, and transionospheric signal propagation (Li et al., 2024). It is important to note that the objective of this study is not to evaluate the storm-time predictability of empirical models; rather, these models are employed as quiet-time baselines to quantify storm-time deviations and interhemispheric differences using distribution-aware metrics (Chou et al., 2023; Peng et al., 2024). During geomagnetic disturbances, interactions between the solar wind and magnetosphere inject energy into the ionosphere–thermosphere system through mechanisms such as particle precipitation, prompt penetration of electric fields (PPEFs) (Tsurutani et al., 2008), and disturbance dynamo currents (Lee et al., 2025; Paul et al., 2025; Venugopal et al., 2025). These drivers disrupt the electrodynamic balance, alter the neutral composition, and modulate global circulation, resulting in significant Total Electron Content (TEC, hereafter VTEC when mapped to the vertical) variability that directly translates into signal delays, phase scintillation, and GNSS service degradation (Aguiar et al., 2025; Bojilova et al., 2024; Li et al., 2024; Yang et al., 2020).

A particularly incisive yet underutilized framework for investigating storm-time dynamics is the analysis of magnetic conjugate points (Förster and Cnossen, 2013; Habarulema et al., 2020; Laundal et al., 2017). These locations, connected by common geomagnetic field lines, offer a natural laboratory for assessing the interhemispheric coupling (Habarulema et al., 2020; Wang et al., 2021). Theoretically, such coupling should result in mirrored ionospheric responses at the conjugate sites. However, empirical studies, including those by Dmitriev et al. (Dmitriev et al., 2017), Habarulema et al. (Habarulema et al., 2020), and Wang et al. (Wang et al., 2021), have demonstrated systematic non-mirrored behavior driven by hemispheric differences in geomagnetic field geometry, dip angle, neutral composition, and thermospheric

https://doi.org/10.5194/egusphere-2025-4594
Preprint. Discussion started: 2 October 2025

winds (Habarulema et al., 2020; Laundal et al., 2017; Wang et al., 2021). Such non-mirrored behaviors are particularly critical for GNSS applications because prediction algorithms often assume hemispheric symmetry. These divergences can exceed approximately 100–150% during intense storms, such as the 2015 St. Patrick's Day event (Astafyeva et al., 2015) and surpassed 200% in the American sector during the August 25–27, 2018 storm, as analyzed in subsequent multi-instrumental and modeling studies (Cherniak and Zakharenkova, 2022; Zhai et al., 2023), resulting in severe and unpredictable GNSS errors. While extreme asymmetries (>200%) have been reported in the American sector during this storm (Cherniak and Zakharenkova, 2022; Zhai et al., 2023), our study focuses on the European, African, and Asian sectors to provide a complementary global perspective and assess whether such severe discrepancies are also prevalent in other longitudinally distinct regions with high user density. Despite their practical importance, conjugate-point discrepancies remain insufficiently quantified in terms of both their physical drivers and their representation in operational models (Cnossen and Förster, 2016; Laundal et al., 2017). Global model validations (e.g., Bilitza et al., 2017 (Bilitza et al., 2017)) often emphasize averaged metrics, whereas regional case studies, such as Sherif et al. (2024) (Sherif et al., 2024), highlight that performance can vary substantially across local longitudinal sectors, underscoring the need for conjugate-point frameworks that explicitly capture hemispheric differences.

Despite the recognized need for improvement, empirical models such as IRI-2016, IRI-Plas, and NeQuick2 continue to serve as standard reference frameworks for ionospheric specifications in GNSS and communication system applications (Chou et al., 2023; Luo et al., 2023; Peng et al., 2024). These models are particularly effective in replicating climatological behavior under quiet time conditions. However, they were not originally developed to account for storm-time electrodynamics (Cnossen and Förster, 2016; Laundal et al., 2017). This limitation has been acknowledged for some time, yet validation studies predominantly focus on global averages or pointwise error statistics, such as RMSE or MAE (Bilitza et al., 2017; Luo et al., 2023; Sherif et al., 2024). Although these metrics effectively quantify magnitude errors, they do not adequately capture distributional differences in TEC variability, structural mismatches across hemispheres, or the storm-phase dependence of model skill (Jiang et al., 2024). Moreover, very few validation efforts have explicitly employed a conjugate-point framework (Astafyeva et al., 2015; Habarulema et al., 2020; Laundal et al., 2017; Wang et al., 2021; Zhai et al., 2023), leaving hemispheric divergence, a critical aspect of storm-time GNSS degradation, largely unexplored.

https://doi.org/10.5194/egusphere-2025-4594
Preprint. Discussion started: 2 October 2025

Utilizing GNSS-derived TEC as a widely recognized benchmark, we employed three complementary validation metrics: (i) Mean Absolute Error (MAE), (ii) root-mean-square error (RMSE), and (iii) distribution-sensitive Kullback–Leibler Divergence (KLD). While MAE and RMSE assess the pointwise accuracy (Bilitza et al., 2017; Tang et al., 2020), KLD evaluates the structural discrepancies between the modeled and observed TEC distributions (Adolfs et al., 2022). In this study, KLD was calculated between the probability distributions of the modeled and observed TEC during the storm phases (initial, main, and recovery) using consistent binning across both datasets (refer to Section 2.4 for implementation details). This metric was specifically selected because of its asymmetry and sensitivity to differences in the tails of distributions, which are essential for identifying storm-time anomalies that manifest as rare but high-impact events in the TEC. Given that the TEC structure directly influences range delay and scintillation risk, distribution-aware validation is operationally pertinent to GNSS integrity (Bojilova et al., 2024; Li et al., 2024; Martinon et al., 2023). Beyond geospace science, similar distribution-sensitive divergence metrics are extensively utilized in wireless communication research to evaluate channel reliability and error propagation (Al-Jarrah et al., 2023; Manimegalai and Bhagyaveni, 2019), highlighting their methodological significance in detecting storm-time TEC anomalies. This cross-disciplinary application underscores the methodological robustness of incorporating KLD into our framework, as both ionospheric TEC variability and wireless channel fluctuations exhibit similar distribution-sensitive error characteristics.

By integrating these approaches, our analysis (i) elucidates the conditions under which empirical models fail during storm forcing, (ii) quantifies cross-hemispheric differences at conjugate locations, and (iii) underscores the methodological benefits of distribution-aware validation for communication-focused applications (Adolfs et al., 2022; Al-Jarrah et al., 2023; Habarulema et al., 2020; Jiang et al., 2024; Luo et al., 2023; Manimegalai and Bhagyaveni, 2019; Wang et al., 2021). In doing so, we reconceptualize the role of empirical ionospheric models in storm-time contexts, not as predictive tools for disturbed conditions, but as reference baselines whose limitations, when properly characterized, provide critical insights into GNSS reliability and wireless system vulnerability. This dual perspective, combining conjugate-point analysis with distribution-sensitive metrics, offers a novel contribution by bridging space weather science and applied wireless communication (Adolfs et al., 2022; Al-Jarrah et al., 2023; Habarulema et al., 2020; Jiang et al., 2024; Luo et al., 2023; Manimegalai and Bhagyaveni, 2019; Wang et al., 2021).

https://doi.org/10.5194/egusphere-2025-4594
Preprint. Discussion started: 2 October 2025

2 Data and Model

This study examines the ionospheric response during a geomagnetic storm from August 25 to 27, 2018, at two pairs of magnetic conjugate stations: Ambalavao (21.9°S, 46.8°E) and Haifa (32.8°N, 35.0°E), representing mid-latitudes, and Malindi (3.0°S, 40.1°E) and Djibouti (11.5°N, 42.9°E), representing low latitudes (Akala et al., 2021; Astafyeva et al., 2022; Piersanti et al., 2020; Zhai et al., 2023). These stations were strategically selected to capture distinct geophysical regimes, facilitating a systematic evaluation of hemispheric asymmetries across both mid- and equatorial latitudes (Förster and Haaland, 2015; Laundal and Richmond, 2017). Figure 1 illustrates the geographic distribution of stations and their conjugate linkages. The East African and Eastern Mediterranean sectors were chosen because of their high density of GNSS users and critical satellite communication routes, making the precise characterization of TEC variability in these regions essential for service reliability (European GNSS Service Centre (GSC), 2015; Ionospheric Correction Algorithms (NeQuick-G / NTCM-G), 2025). This configuration is particularly pertinent for GNSS users because spatial and hemispheric variability in the TEC directly results in positioning errors, signal delays, and service degradation in wireless communication systems.

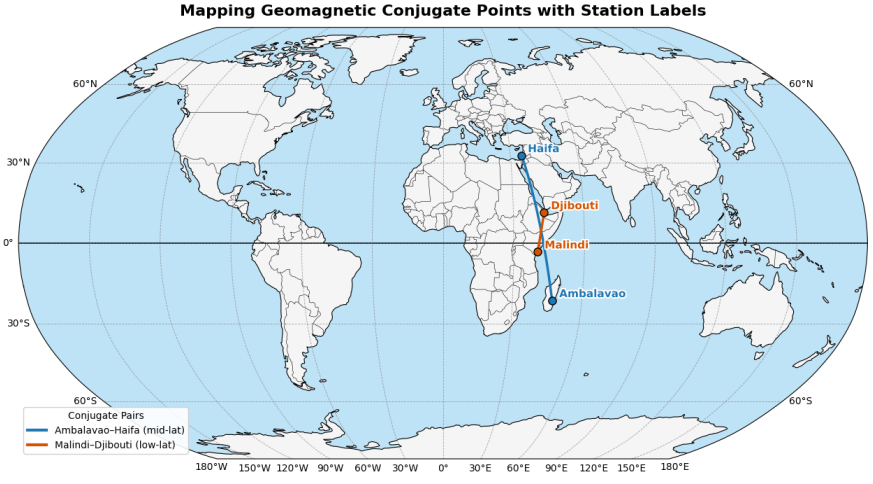

Fig. 1 Geographic distribution of GNSS stations and their corresponding magnetic conjugate links. Station identifiers (IGS codes) are indicated, and great-circle arcs are utilized to approximate the connectivity of the geomagnetic field lines. The latitude and longitude graticules were presented at intervals of 20°.

2.1 Observational Data

https://doi.org/10.5194/egusphere-2025-4594
Preprint. Discussion started: 2 October 2025

Total Electron Content (TEC) was derived from dual-frequency GNSS data obtained via the International GNSS Service (IGS). RINEX-format observations from GPS, GLONASS, and Galileo satellites (when available) were processed at a 30-second resolution using the IONOLAB-TEC software suite (Sezen et al., 2013). For each epoch, all satellite–receiver links above a 30° elevation mask were included. The vertical TEC (VTEC) values were computed per satellite at the ionospheric pierce point and subsequently averaged to obtain a station-level time series, thereby reducing satellite-specific noise while retaining the storm-time variability most relevant to the GNSS navigation accuracy.

To ensure calibration accuracy, the IONOLAB-BIAS algorithm was employed to estimate and eliminate differential code biases (DCBs) from both receivers and satellites (Arikan et al., 2008). This process incorporates precise IGS orbits and IONEX-derived global DCB products (Hernández-Pajares et al., 2009). The methodology has undergone extensive validation against global IGS centers, and is recognized for providing reliable single-station TEC retrievals under both quiet and disturbed conditions. Although GNSS-derived TEC is widely regarded as the reference ground truth, it is important to acknowledge the limitations associated with receiver biases, multipaths, and calibration errors. These effects were mitigated through IONOLAB-BIAS correction and validated orbits/DCB products, ensuring that the residual errors were minimal relative to the storm-time TEC variability of interest in this study, as supported by the comprehensive validation of IONOLAB methodology against global IGS products (Sezen et al., 2013). Station metadata, receiver types, and data availability windows are summarized in Table S1 (Supplementary Information).

2.2 Empirical Models

Three widely used empirical ionospheric models were selected for this study: IRI-2016, IRI-Plas, and NeQuick2 (Bilitza et al., 2017; Gulyaeva et al., 2011; Nava et al., 2008). These models are not intended as predictive tools for storm-time conditions, as they were not designed for such purposes. Instead, they serve as climatological baselines, against which deviations during storm-time and hemispheric asymmetries can be systematically quantified. From the perspective of wireless communication, these models are frequently integrated into GNSS error correction, integrity monitoring, and service reliability assessments, rendering their evaluation particularly pertinent under disturbed conditions (European GNSS Service Centre (GSC), 2015; Ionospheric Correction Algorithms (NeQuick-G / NTCM-G), 2025).

IRI-2016 represents the climatological monthly medians of ionospheric parameters (Bilitza et al., 2017). IRI-Plas extends IRI by incorporating plasmaspheric contributions to the

https://doi.org/10.5194/egusphere-2025-4594
Preprint. Discussion started: 2 October 2025

Total Electron Content (TEC), thereby enhancing the representation of the topside ionosphere (Gulyaeva et al., 2011). NeQuick2 is a semi-empirical model driven by solar flux inputs (F10.7, or the effective ionization level, Az) to adjust the electron density profiles dynamically (Nava et al., 2008). Although storm-time empirical models exist (e.g., the IRI-based STORM extension) (Araujo-Pradere et al., 2002), this study specifically focuses on the performance of the standard, unmodified versions of IRI-2016, IRI-Plas, and NeQuick2. These standard versions are the most widely implemented in operational GNSS receivers and communication systems for real-time error correction. Therefore, evaluating their inherent limitations during storms is of direct practical relevance (European GNSS Service Centre (GSC), 2015; Ionospheric Correction Algorithms (NeQuick-G / NTCM-G), 2025).

2.3 Storm Phases

Model outputs and GNSS observations were systematically compared across three distinct storm phases, initial, main, and recovery, as defined by the temporal variation in the Dst index (Gonzalez et al., 1994). This phase-resolved methodology facilitates the assessment of model performance in relation to storm progression, rather than averaging results across dynamically disparate intervals. This distinction is crucial for relevance to communication systems, as GNSS errors typically reach their peak during the main phases and stabilize during the recovery phase.

2.4 Statistical Metrics

Three statistical measures were employed to assess the model performance relative to GNSS-derived TEC:

$$MAE = \frac{1}{n}\sum_{i=1}^{n}\left|TEC_i - TEC_p\right| \quad (1)$$

$$RMSE = \sqrt{\frac{1}{n}\sum_{i=1}^{n}\left(TEC_i - TEC_p\right)^2} \quad (2)$$

where TEC_i is the observed value, TEC_p the model output, and n the number of samples. Equations (1) and (2) capture pointwise errors, with MAE emphasizing the average deviations and RMSE amplifying larger mismatches.

To go beyond magnitude-based errors, we introduced the Kullback–Leibler Divergence (KLD):

$$KLD = \sum_i P(i) log \frac{P(i)}{Q(i)} \quad (3)$$

https://doi.org/10.5194/egusphere-2025-4594
Preprint. Discussion started: 2 October 2025

In this context, P(i) and Q(i) denote the probability distributions of the observed and modeled Total Electron Content (TEC), respectively, with the divergence of the model distribution Q from the observed distribution P being the focus. A lower Kullback-Leibler divergence (KLD) signifies closer alignment in the distributional structure. Unlike Equations (1) and (2), Equation (3) is sensitive to discrepancies in variance, skewness, and multimodality, which often become pronounced during storm-time dynamics (Kullback and Leibler, 1951; Sason and Verdu, 2016). For implementation, probability distributions were estimated using histograms with bin widths determined by the Freedman–Diaconis rule to ensure consistency across datasets (Freedman and Diaconis, 1981). Kernel density estimation (KDE) was also evaluated as part of a comprehensive sensitivity analysis. To prevent undefined values in the logarithmic term, a small smoothing constant ($\varepsilon \approx 10^{-6}$) was added to all bins following standard divergence-analysis practice (Cover and Thomas, 2005). This setup is also consistent with wireless communication research, where divergence metrics are commonly applied to evaluate the channel reliability and error propagation.

A comprehensive sensitivity analysis was performed to evaluate the robustness of the Kullback-Leibler divergence (KLD) metric in relation to the inherent subjectivity of probability density estimation. KLD was recalculated for each station-model pair across a broad spectrum of histogram bin counts (ranging from 20 to 60) and Gaussian kernel density estimation (KDE) bandwidths (spanning 0.30 to 0.70 TECU). Variability in the results was quantified using the relative percentage change (Δ%) across these parameter ranges. This analysis demonstrated that KLD is systematically sensitive to these parameters; it generally increases with finer histogram binning and decreases with broader KDE smoothing. Importantly, the extent of this sensitivity is highly contingent on both the model and the geophysical location.

Across all stations, the Δ bin values ranged from 3.68% to 75.64%, whereas the Δ_KDE values varied from 10.85% to 67.23%. The mid-latitude stations, Ambalavao and Djibouti, exhibited significant sensitivity, with the KLD increasing consistently with finer binning (Δ_bins ≈ 61–67% across models) and decreasing with broader KDE smoothing (Δ_KDE ≈ 56–64% at Ambalavao; 11–58% at Djibouti). Haifa demonstrated the highest parameter sensitivity, particularly for NeQuick2 (Δ_bins ≈ 75.6%, Δ_KDE ≈ 67.2%), whereas IRI-PLAS remained relatively stable at this location (Δ_bins ≈ 35.8%, Δ_KDE ≈ 30.0%). Conversely, the equatorial station Malindi was an outlier; its long-tailed PDFs rendered the KLD nearly insensitive to binning (Δ_bins ≈ 3–7% across models), although it remained responsive to the KDE bandwidth (Δ_KDE ≈ 45–48% for IRI-PLAS and NeQuick2).

https://doi.org/10.5194/egusphere-2025-4594
Preprint. Discussion started: 2 October 2025

Crucially, the divergence between the model and observations remained consistent across all parameter configurations. Consequently, our conclusions based on KLD are indicative of authentic structural differences rather than artifacts arising from histogram or KDE settings. The comprehensive results of this sensitivity analysis are presented in Supplementary Figures S1-S12 and summarized in Supplementary Table S2. This thorough validation emphasizes the robustness of our distribution-aware evaluation and offers an essential context for interpreting the KLD results discussed in the subsequent sections.

2.5 Theoretical Framework

Conjugate-point analysis is based on storm-time electrodynamics. Prompt penetration electric fields (PPEFs) and disturbance dynamo currents facilitate large-scale plasma redistribution along the magnetic field lines (Blanc and Richmond, 1980; Tsurutani et al., 2008). Although theoretical models anticipate mirrored behaviors at conjugate points, empirical observations consistently reveal hemispheric asymmetries owing to geomagnetic field geometry, conductivity imbalances, and neutral wind filtering (Förster and Haaland, 2015; Laundal and Richmond, 2017). Total Electron Content (TEC) serves as a crucial diagnostic tool for these processes, and its distribution across hemispheres provides a rigorous test for empirical models. Beyond its geophysical importance, this framework elucidates the mechanisms by which ionospheric storms impair Global Navigation Satellite System (GNSS) positioning accuracy and communication reliability, underscoring the necessity of cross-disciplinary evaluation methods. The theoretical expectation of both coupling and asymmetry directly informs our methodological choices: selecting conjugate pairs offers a controlled experimental setup, whereas the Kullback-Leibler divergence (KLD) metric is particularly suited for detecting the non-mirrored distributional differences predicted by theory (Bilitza et al., 2017). Consequently, our framework provides a direct observational test for these electrodynamic principles. Therefore, precise quantification of hemispheric divergence, a critical factor in storm-time GNSS degradation, remains a central challenge, emphasizing the need for conjugate-point validation frameworks. As conjugate sites do not share a common local time (LT) at a given UT, the interpretation of hemispheric asymmetry is potentially confounded by diurnal illumination. In future analyses, we will employ LT-aligned comparisons and explicit LT controls to isolate electrodynamic coupling from diurnal effects.

3 Results

3.1 Storm Overview and Ionospheric Context

https://doi.org/10.5194/egusphere-2025-4594
Preprint. Discussion started: 2 October 2025

The geomagnetic storm examined in this study occurred between August 25 and 27, 2018 and exhibited characteristics of a moderately intense to strong event. As illustrated in Figure 2, Dst reached −176 nT, Kp peaked at 7.3, and ap increased to 154 nT (Piersanti et al., 2020). The main phase, characterized by a prolonged southward turning of the IMF Bz, extended from 18:00 UT on August 25 to 06:00 UT on August 26 (Piersanti et al., 2020). Taken together, these indicators are consistent with strong storm conditions (Piersanti et al., 2020).

Storm classifications vary in the literature. Akala et al. (2021) documented that the geomagnetic activity on August 26, 2018, was consistent with a G3-level event precipitated by a solar filament eruption on August 20 (Akala et al., 2021). Subsequent analyses suggested that the storm was predominantly influenced by weak CME transients interacting with Corotating Interaction Regions (CIRs) and High-Speed Streams (HSSs) rather than by a strong magnetic cloud, which is typically associated with severe geomagnetic disturbances (Akala et al., 2021; Gonzalez et al., 2011).

Although Prompt Penetration Electric Fields (PPEFs) were relatively modest (≈0.3 mV/m; Akala et al., 2021) (Akala et al., 2021), our observations reveal significant ionospheric responses, particularly in the form of pronounced Total Electron Content (TEC) deviations at magnetic conjugate points. This underscores two critical aspects: (i) even moderately driven storms with sustained southward Interplanetary Magnetic Field (IMF) Bz can induce strong interhemispheric ionospheric coupling and (ii) localized spatial variability plays a decisive role in shaping storm-time ionospheric impacts.

Consequently, while the August 2018 event may not be classified as an extreme storm based on solar drivers, its impact on the ionosphere serves as a valuable case study for assessing the performance of the empirical model under disturbed and complex geomagnetic conditions. This perspective is consistent with previous research indicating that even G2–G3 storms can significantly disrupt GNSS positioning and communication systems when they occur under favorable local time and background thermospheric conditions (Valdés-Abreu et al., 2021; Xue et al., 2024).

https://doi.org/10.5194/egusphere-2025-4594
Preprint. Discussion started: 2 October 2025

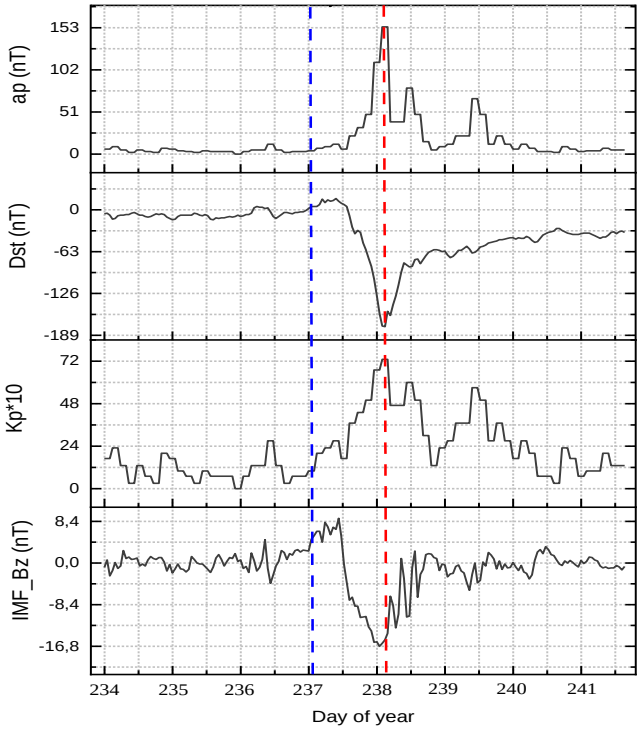

Fig. 2 Temporal variations in the IMF Bz, Dst, Kp, and ap indices observed from August 22 to 29, 2018. The main phase of the storm, which occurred from August 25, 18:00 UT to August 26, 06:00 UT, is delineated by the vertical dashed lines. A pronounced minimum in the Dst index and sustained southward orientation of the IMF Bz corroborated the intensity of the storm.

3.2 TEC Model Evaluation at Conjugate Points

To assess the efficacy of empirical ionospheric models in representing storm-time dynamics, we conducted a comparative analysis of NeQuick2, IRI-2016, and IRI-Plas during a geomagnetic storm that occurred from August 25 to 27, 2018. This evaluation concentrated on two magnetic conjugate station pairs, Ambalavao–Haifa and Malindi–Djibouti, encompassing both mid-latitude and equatorial responses. Model outputs were systematically compared with GNSS-derived Total Electron Content (TEC) using three complementary metrics: MAE, RMSE, and KLD. This hybrid framework, which integrates magnitude-based errors with distribution-sensitive divergence, offers a comprehensive assessment of the model performance across various storm phases. This approach is particularly valuable given the nonlinear, asymmetric, and rapidly evolving nature of ionospheric disturbances during geomagnetic

https://doi.org/10.5194/egusphere-2025-4594
Preprint. Discussion started: 2 October 2025

storms, particularly when interhemispheric processes are considered (Bilitza et al., 2017; Cherniak and Zakharenkova, 2019; Vankadara et al., 2022).

Although these empirical models are extensively employed for climatological specifications, they possess inherent limitations in accurately representing the rapid electrodynamic processes that occur during geomagnetic disturbances. These processes include the prompt penetration of electric fields, storm-time thermospheric wind surges, and hemispheric conductivity gradients (Blanc and Richmond, 1980; Tsurutani et al., 2008).

3.2.1 Ambalavao–Haifa pair: How do the models behave at mid-latitudes?

As illustrated in Table 1, all three models demonstrated optimal performance during the recovery phase, with NeQuick2 exhibiting the lowest errors (MAE ≈ 0.4 TECU; RMSE ≈ 1.0 TECU). Conversely, the error rates increased significantly during the main phase, particularly for IRI-2016 (while IRI-Plas occasionally yielded a smaller MAE at mid-latitudes during the MP; Table 1), highlighting their limited capacity to accurately capture rapid storm-time fluctuations. These findings align with previous reports indicating that IRI models tend to underestimate the daytime TEC and oversimplify storm variability (Bilitza et al., 2017; Cherniak and Zakharenkova, 2019; Endeshaw, 2020; Gulyaeva et al., 2011).

Table 1 TEC model performance for Ambalavao–Haifa across storm phases (BP, MP, and RP), errors (MAE, RMSE, and TECU), and divergence (KLD; –) are reported relative to OBS |ΔTEC|.

Metric	Phase	Observed (Amb–Haifa)	NeQuick2	IRI-2016	IRI-Plas
MAE (TECU)	BP	6.0	1.7	1.8	2.1
	MP	6.2	2.8	2.3	1.3
	RP	2.3	0.4	0.5	1.5
RMSE (TECU)	BP	6.4	1.9	2.1	2.8
	MP	6.4	3.0	2.5	1.7
	RP	4.2	1.0	1.3	3.5
KLD (–)	BP	0.08	0.30	0.31	0.17
	MP	0.07	0.22	0.26	0.13
	RP	0.16	0.26	0.31	0.16

Note: MAE and RMSE are in TECU, and KLD is dimensionless.

An important insight derived from the Kullback–Leibler Divergence (KLD) is that elevated values during the initial phase indicate that despite a moderate Mean Absolute Error (MAE) and Root Mean Square Error (RMSE), the models inaccurately represented the statistical structure of the Total Electron Content (TEC) distribution. Variance, skewness, and tail behavior, which are often obscured by pointwise metrics, have proven crucial in capturing the onset of storm-driven changes (Arikan et al., 2016; Karatay et al., 2010). To our knowledge, this is among the earliest distribution-aware (KLD) validations explicitly framed within a conjugate-point analysis for this storm and station set.

https://doi.org/10.5194/egusphere-2025-4594
Preprint. Discussion started: 2 October 2025

3.2.2 Haifa–Ambalavao Reverse Evaluation: The Hemispheric Disconnect

Upon reversing the evaluation to compare Haifa with Ambalavao, distinct hemispheric asymmetry was evident (Table 2). Errors were consistently more pronounced at the Northern Hemisphere site, particularly during the main phase, suggesting increased modeling challenges at higher northern mid-latitudes. This phenomenon aligns with variations in the seasonal solar illumination, geomagnetic field geometry, and background electron density gradients (Laundal et al., 2017; Mendillo, 2006).

Table 2 Directional (reverse) evaluation for Haifa–Ambalavao across BP, MP, RP; errors (MAE, RMSE; TECU) and divergence (KLD; –) reported relative to OBS |ΔTEC|.

Metric	Phase	Observed (Haifa–Amb)	NeQuick2	IRI-2016	IRI-Plas
MAE (TECU)	BP	6.0	2.8	4.3	2.3
	MP	6.2	4.6	6.6	2.6
	RP	2.3	0.5	1.2	0.7
RMSE (TECU)	BP	6.4	3.3	4.8	2.8
	MP	6.4	4.7	6.7	2.9
	RP	4.2	1.2	2.2	1.4
KLD (–)	BP	0.08	0.04	0.05	0.03
	MP	0.07	0.08	0.07	0.06
	RP	0.16	0.11	0.07	0.10

Note: MAE and RMSE are in TECU, and KLD is dimensionless.

The Kullback-Leibler divergence (KLD) further accentuates the asymmetry, indicating that the models encountered difficulties with the statistical structure of Total Electron Content (TEC) distributions in Haifa, beyond merely the mean errors.

3.2.3 Malindi–Djibouti Pair: The Challenge of the Equator

For the Malindi–Djibouti pair, performance declined further (Table 3). During the main phase, the IRI-2016 model exhibited a Mean Absolute Error (MAE) exceeding 15 Total Electron Content Units (TECU), with a Root Mean Square Error (RMSE) approaching 16 TECU, which is significantly larger than the errors observed at mid-latitudes. These discrepancies underscore the inherent complexity of the equatorial ionosphere, which is significantly influenced by the Equatorial Ionization Anomaly (EIA), neutral wind reversal, and storm-time coupling processes (Cherniak and Zakharenkova, 2022; Zhang et al., 2021).

Table 3 TEC model performance for Djibouti–Malindi across BP, MP, and RP; errors (MAE, RMSE, TECU) and divergence (KLD; –) reported relative to OBS |ΔTEC|.

Metric	Phase	Observed (Mal–Dji)	NeQuick2	IRI-2016	IRI-Plas
MAE (TECU)	BP	12.5	10.5	10.9	5.5
	MP	13.3	15.7	15.2	8.1
	RP	5.3	5.0	4.8	2.4
RMSE (TECU)	BP	12.9	11.1	11.5	7.2
	MP	14.0	15.9	15.2	8.6

https://doi.org/10.5194/egusphere-2025-4594
Preprint. Discussion started: 2 October 2025

	RP	8.9	8.6	8.2	4.7
KLD (–)	BP	0.10	0.23	0.28	0.15
	MP	0.14	0.13	0.17	0.09
	RP	0.07	0.14	0.16	0.09

Note: MAE and RMSE are in TECU, and KLD is dimensionless.

The KLD values indicate that the model not only inaccurately estimated TEC magnitudes, but also failed to maintain distributional characteristics, emphasizing the specific challenges associated with equatorial dynamics.

3.2.4 NeQuick2's Edge in the Recovery Phase

Despite its recognized limitations, NeQuick2 consistently surpassed IRI-2016 and IRI-Plas during the recovery phase, as shown in Table 4. With mean absolute error (MAE) values below 1 total electron content unit (TECU), relatively low root mean square error (RMSE), and Kullback-Leibler divergence (KLD), NeQuick2 demonstrated considerable robustness once the ionosphere stabilized following the peak disturbance (Montenbruck and González Rodríguez, 2020; Nava et al., 2008).

Table 4 Directional (reverse) evaluation for Malindi–Djibouti across BP, MP, and RP; errors (MAE, RMSE, TECU) and divergence (KLD; –) reported relative to OBS |ΔTEC|.

Metric	Phase	Observed (Mal–Dji)	NeQuick2	IRI-2016	IRI-Plas
MAE (TECU)	BP	12.5	3.9	4.2	10.7
	MP	13.3	2.9	3.3	8.7
	RP	5.28	0.7	1.2	3.8
RMSE (TECU)	BP	12.92	5.0	5.2	12.2
	MP	13.9	4.2	3.8	10.2
	RP	8.9	1.5	2.6	7.3
KLD (–)	BP	0.10	0.23	0.28	0.15
	MP	0.14	0.13	0.17	0.09
	RP	0.17	0.14	0.16	0.09

Note: MAE and RMSE are in TECU, and KLD is dimensionless.

The KLD values remained relatively low, indicating that NeQuick2 maintained its structural integrity during the recovery. This relative success is likely attributable to its solar-flux-driven parameterization, which facilitates dynamic adjustment during recovery, in contrast to IRI-based models that rely on climatological medians and lack flexibility. However, NeQuick2's simplified plasmaspheric representation resulted in an underestimation of the topside TEC (Cherniak and Zakharenkova, 2019), highlighting that even the most reliable empirical models have inherent limitations under storm conditions (Kashcheyev and Nava, 2019; Pezzopane et al., 2023; Pezzopane and Pignalberi, 2019).

4 Discussion

4.1 Model Limitations and Benchmark Role

https://doi.org/10.5194/egusphere-2025-4594
Preprint. Discussion started: 2 October 2025

In this study, empirical models were employed as baselines for quiet-time conditions to assess deviations during storm periods; however, they were not used as predictors of storm events. This analysis underscores a well-established limitation: empirical ionospheric models such as IRI-2016, IRI-Plas, and NeQuick2 are not designed to predict storm-time phenomena (Bilitza et al., 2017; Gulyaeva et al., 2011; Nava et al., 2008). These models are based on climatological averages and are not intended to capture transient electrodynamic forcings (Bilitza et al., 2017; Blanc and Richmond, 1980; Nava et al., 2008). Rather than viewing this as a deficiency, our study reinterprets their function by providing benchmarks for quiet-time conditions against which storm-time deviations can be systematically quantified. Extensions such as the IRI-based STORM module aim to parameterize storm effects; however, they remain constrained by the complexity of magnetosphere–ionosphere–thermosphere interactions (Araujo-Pradere et al., 2002; Astafyeva et al., 2015; Blanc and Richmond, 1980). Therefore, evaluating baseline empirical models under storm conditions is scientifically valuable not as a test of forecasting ability but as a means to diagnose where physical processes diverge from climatological assumptions (Bilitza et al., 2017; Gulyaeva et al., 2011). Notably, IRI-Plas occasionally exhibited lower magnitude errors (MAE/RMSE) during the main phase at mid-latitudes (e.g., Tables 1 and 2), which may have resulted from its plasmaspheric extension stabilizing topside contributions under certain conditions or from differences in parameterization. This occasionally lower MAE/RMSE during the main phase is physically plausible: the plasmaspheric extension can partially stabilize topside contributions and reduce magnitude errors when the scale heights increase rapidly. However, this advantage does not consistently translate into superior distributional fidelity, as indicated by the KLD, underscoring that IRI-Plas may match totals while still misrepresenting variance, skewness, or tails. However, establishing generality requires further case studies (Arikan et al., 2016; Gulyaeva et al., 2011).

4.2 Hemispheric Asymmetry and Physical Insights

One of the most evident outcomes is the pronounced hemispheric asymmetry observed at the conjugate points, notably in the Malindi–Djibouti pair. Despite their magnetic linkage, these sites exhibited significantly different TEC signatures during the main phase, with IRI-2016 errors exceeding 15 TECU at Djibouti. This asymmetry cannot be attributed solely to model deficiencies; it reflects genuine geophysical influences, including solar illumination gradients, thermospheric wind circulation, and geographic offsets (Cnossen and Förster, 2016; Förster and Cnossen, 2013; Förster and Haaland, 2015; Laundal et al., 2017; Laundal and Richmond, 2017). These findings are consistent with previous reports on conjugate divergence

https://doi.org/10.5194/egusphere-2025-4594
Preprint. Discussion started: 2 October 2025

and underscore the necessity for conjugate frameworks in future validation studies because assumptions of symmetry obscure significant physical variability (Cherniak and Zakharenkova, 2022; Habarulema et al., 2020; Zhang et al., 2021). Although the hemispheric asymmetries discussed above reflect authentic geophysical drivers, conjugate sites do not share the same local time (LT) at a given UT. Because TEC is strongly influenced by solar illumination (LT), a portion of the observed divergence may result from LT offsets rather than solely from hemispheric electrodynamics. Future analyses should incorporate LT-aligned composites or explicit LT controls to isolate this contribution, which represents a limitation of this study (Cnossen and Förster, 2016; Förster and Cnossen, 2013; Förster and Haaland, 2015; Laundal et al., 2017; Laundal and Richmond, 2017; Mendillo, 2006).

4.3 Structural Reliability via KLD

Traditional error metrics, such as the Mean Absolute Error (MAE) and Root Mean Square Error (RMSE), evaluate the mean accuracy but do not ascertain whether the statistical structure of storm-time Total Electron Content (TEC) is preserved. By utilizing the Kullback–Leibler Divergence (KLD), we identified instances where models appeared satisfactory in terms of mean error yet inaccurately represented variance, skewness, or distribution tails, particularly at the onset of storms (Arikan et al., 2016; Karatay et al., 2010; Kullback and Leibler, 1951). This distinction is significant; a model that accurately predicts numerical values may still inadequately capture the dynamics governing ionospheric variability. Our findings demonstrate that KLD complements conventional metrics by revealing hidden discrepancies in model performance (Arikan et al., 2016; Cover and Thomas, 2005; Karatay et al., 2010; Kullback and Leibler, 1951; Sason and Verdu, 2016). The application of KLD to conjugate-point analysis represents a methodological advancement beyond standard evaluation (Kullback and Leibler, 1951; Sason and Verdu, 2016). Operationally, an elevated KLD indicates that the model underrepresents the distribution tails that drive rare but high-impact TEC excursions, which are the most challenging for Global Navigation Satellite System (GNSS) correction/integrity and wireless links. It is important to note that KLD quantifies the similarity of distributional shape (variance, skewness, multimodality) rather than the absolute magnitude of errors; thus, a station can exhibit large MAE/RMSE yet moderate KLD if the modeled distribution preserves shape, whereas smaller magnitude errors can still yield higher KLD when the distributional structure is incorrect—hence our joint reporting of MAE/RMSE and KLD.

Sensitivity analyses (Supplementary Figs. S1–S12; Tables S1–S2) confirm that these conclusions are not artifacts of density estimation settings. The analysis revealed that NeQuick2

https://doi.org/10.5194/egusphere-2025-4594
Preprint. Discussion started: 2 October 2025

was the most parameter-sensitive model, as indicated by the significant fluctuations in the KLD values depending on the bin count and KDE bandwidth. In contrast, IRI-Plas demonstrated greater stability. This finding underscores that distribution-aware metrics not only identify structural discrepancies but also highlight the vulnerability of different models to methodological assumptions. Therefore, distribution-aware metrics are directly relevant to risk-focused validation (Al-Jarrah et al., 2023; Kullback and Leibler, 1951; Manimegalai and Bhagyaveni, 2019; Sason and Verdu, 2016).

4.4 Future Directions

The degradation observed during storm-time was most pronounced during the main phase, wherein all models failed to accurately capture rapid electrodynamic forcing(Astafyeva et al., 2015, 2022). Conversely, the recovery phase exhibited variability contingent upon the model used, with NeQuick2 demonstrating a relative advantage (Cherniak and Zakharenkova, 2019; Kashcheyev and Nava, 2019; Montenbruck and González Rodríguez, 2020; Pezzopane et al., 2023; Pezzopane and Pignalberi, 2019). This disparity underscores the necessity of developing models capable of dynamic adaptation across different phases rather than relying on static climatological assumptions (Adolfs et al., 2022; Jiang et al., 2024; Luo et al., 2023).

The most pronounced cross-hemispheric divergences are observed at equatorial conjugate pairs, where complex factors such as pre-reversal enhancement (Fejer, 2002), EIA modulation, and neutral wind asymmetries intensify the discrepancies between models and observations (Cherniak and Zakharenkova, 2022; Cnossen and Förster, 2016; Habarulema et al., 2020; Wang et al., 2021). These findings highlight the limitations of climatological baselines and emphasize the necessity of incorporating storm-responsive physical processes.

The utilization of the Kullback–Leibler Divergence (KLD) presents notable diagnostic benefits by detecting structural errors such as variance inflation, skewness shifts, and tail distortions, which are not identified by MAE and RMSE (Al-Jarrah et al., 2023; Cover and Thomas, 2005; Freedman and Diaconis, 1981; Kullback and Leibler, 1951; Manimegalai and Bhagyaveni, 2019; Sason and Verdu, 2016). This highlights the importance of adopting distribution-aware metrics as the standard in storm-time validation, particularly in applications where communication is of critical importance.

These findings collectively highlight the imperative for the development of hybrid or data-assimilative models that integrate solar-wind coupling, E×B drifts (Fejer, 2002), and variations in thermospheric composition. These models must be evaluated using both

https://doi.org/10.5194/egusphere-2025-4594
Preprint. Discussion started: 2 October 2025

magnitude-based and distribution-sensitive metrics (Adolfs et al., 2022; Astafyeva et al., 2015; Jiang et al., 2024; Luo et al., 2023; Tang et al., 2020; Tsurutani et al., 2008). Such approaches are vital for advancing our ability to accurately model storm-time ionospheric dynamics and enhance the reliability of GNSS-enabled systems.

5 Conclusion

By integrating a conjugate-point framework with distribution-aware validation (KLD), this study provides a novel benchmark for assessing empirical ionospheric models during geomagnetic storms. We utilized empirical ionospheric models as baselines for quiet-time conditions to quantify deviations during storm periods at magnetic conjugate points by employing the Mean Absolute Error (MAE), Root Mean Square Error (RMSE), and distribution-aware Kullback–Leibler Divergence (KLD). The analysis of the storm from August 25 to 27, 2018, indicated that the performance of the models was significantly contingent upon the storm phase; all models exhibited degradation during the main phase, with NeQuick2 demonstrating superior performance during the recovery phase. Pronounced hemispheric asymmetries were observed; errors were more substantial, and distributions were more distorted at northern mid-latitudes (Haifa), particularly at the equator (Malindi–Djibouti), reflecting genuine geophysical influences such as illumination, winds, and magnetic geometry.

The Kullback-Leibler Divergence (KLD) effectively identified structural discrepancies, including variance, skewness, and tails, which remained undetected when the Mean Absolute Error (MAE) or Root Mean Square Error (RMSE) appeared moderate. For instance, during the initial phase of the storm at mid-latitudes, KLD revealed significant distributional distortions in the models (e.g., KLD=0.30 for NeQuick2 in Table 1) that were not apparent from the magnitude errors alone (MAE=1.7 TECU), highlighting its critical diagnostic value. This underscores the importance of communication-oriented validations. While NeQuick2's solar-flux parameterization offers certain relative advantages, its topside limitations highlight the fact that no empirical model can fully capture storm-time dynamics.

Crucially, the robustness checks conducted through the sensitivity analysis (Supplementary Figures S1–S12, Table S2) substantiate that these conclusions are not mere artifacts of parameter selection but rather reflect authentic structural discrepancies.

The findings indicate that empirical models should be considered as reference benchmarks rather than predictors. When combined with structure-aware validation, the conjugate-point framework provides a practical methodology for identifying failure modes,

https://doi.org/10.5194/egusphere-2025-4594
Preprint. Discussion started: 2 October 2025

prioritizing physical processes for assimilation, and ultimately enhancing the resilience of GNSS and wireless systems under geomagnetic disturbances. This is particularly relevant across magnetically conjugate links, where asymmetries are the most operationally significant.

While the current study focused on storms occurring from August 25 to 27, 2018, future research will expand this conjugate-point KLD framework to a statistical ensemble of storms across different seasons and phases of the solar cycle to ascertain the generalizability of the findings.

Code availability

Not applicable. This study used standard Python libraries (NumPy, Pandas, Matplotlib) for data analysis and visualization. No custom code has been archived for public release.

Data availability

Solar wind data are provided by the NASA OMNIWeb database (https://omniweb.gsfc.nasa.gov; NASA, 2025). GNSS-derived Total Electron Content (TEC) data were obtained from the International GNSS Service (IGS, https://igs.org) and associated global data centers. Processed datasets used in this study, including storm-event subsets for Ambalavao, Djibouti, Haifa, and Malindi stations, are archived at Zenodo and publicly available (DOI: https://doi.org/10.5281/zenodo.15845821; Korlaelci et al., 2025).

Interactive computing environment

Not applicable.

Sample availability

Not applicable.

Video supplement

Not applicable.

Supplement link

The link to the supplement will be included by Copernicus, if applicable.

Author contributions

Serhat Korlaelci designed the study, developed the methodology, performed the analysis, and prepared the manuscript. Ramazan Atici contributed to data curation, visualization, and

https://doi.org/10.5194/egusphere-2025-4594
Preprint. Discussion started: 2 October 2025

validation. Selçuk Sagir contributed to investigation and writing – review & editing. All authors discussed the results and approved the final manuscript.

Competing interests

The authors declare that they have no conflict of interest.

Disclaimer

Publisher's note: Copernicus Publications remains neutral with regard to jurisdictional claims in published maps and institutional affiliations.

Acknowledgements

The authors acknowledge the use of GNSS data provided by the International GNSS Service (IGS) and the OMNI solar wind database maintained by NASA. We thank Muş Alparslan University for institutional support. The authors used AI-assisted language editing (e.g., ChatGPT by OpenAI) to improve readability. The scientific content and conclusions are entirely the authors. No data analysis or figure generation was performed by AI, and no confidential or personal data were shared with the tool.

Financial support

This research received no external funding.

References

Adolfs, M., Hoque, M. M., and Shprits, Y. Y.: Storm-time relative total electron content modelling using machine learning techniques, Remote Sens., 14, 6155, https://doi.org/10.3390/rs14236155, 2022.

Aguiar, C. R., Monico, J. F. G., and Moraes, A. O.: Impact of ionospheric scintillations on GNSS availability and precise positioning, Space Weather, 23, e2024SW004217, https://doi.org/10.1029/2024SW004217, 2025.

Akala, A. O., Oyedokun, O. J., Amaechi, P. O., Simi, K. G., Ogwala, A., and Arowolo, O. A.: Solar origins of August 26, 2018 geomagnetic storm: Responses of the interplanetary medium and equatorial/low-latitude ionosphere to the storm, Space Weather, 19, e2021SW002734, https://doi.org/10.1029/2021SW002734, 2021.

Al-Jarrah, M., Alsusa, E., and Masouros, C.: A unified performance framework for integrated sensing-communications based on KL-divergence, IEEE Trans. Wirel. Commun., 22, 9390–9411, https://doi.org/10.1109/TWC.2023.3270390, 2023.

Araujo-Pradere, E. A., Fuller-Rowell, T. J., and Codrescu, M. V.: STORM: An empirical storm-time ionospheric correction model 1. Model description, Radio Sci., 37, https://doi.org/10.1029/2001RS002467, 2002.

https://doi.org/10.5194/egusphere-2025-4594
Preprint. Discussion started: 2 October 2025

588 Arikan, F., Nayir, H., Sezen, U., and Arikan, O.: Estimation of single station interfrequency
589 receiver bias using GPS-TEC, Radio Sci., 43, 2007RS003785,
590 https://doi.org/10.1029/2007RS003785, 2008.

591 Arikan, F., Shukurov, S., Tuna, H., Arikan, O., and Gulyaeva, T. L.: Performance of GPS slant
592 total electron content and IRI-Plas-STEC for days with ionospheric disturbance, Geod.
593 Geodyn., 7, 1–10, https://doi.org/10.1016/j.geog.2015.12.009, 2016.

594 Astafyeva, E., Zakharenkova, I., and Förster, M.: Ionospheric response to the 2015 St. Patrick's
595 Day storm: A global multi-instrumental overview, J. Geophys. Res. Space Phys., 120, 9023–
596 9037, https://doi.org/10.1002/2015JA021629, 2015.

597 Astafyeva, E., Yasyukevich, Y. V., Maletckii, B., Oinats, A., Vesnin, A., Yasyukevich, A. S.,
598 Syrovatskii, S., and Guendouz, N.: Ionospheric disturbances and irregularities during the 25–
599 26 August 2018 geomagnetic storm, J. Geophys. Res. Space Phys., 127, e2021JA029843,
600 https://doi.org/10.1029/2021JA029843, 2022.

601 Bilitza, D., Altadill, D., Truhlik, V., Shubin, V., Galkin, I., Reinisch, B., and Huang, X.:
602 International reference ionosphere 2016: From ionospheric climate to real-time weather
603 predictions, Space Weather, 15, 418–429, https://doi.org/10.1002/2016SW001593, 2017.

604 Blanc, M. and Richmond, A. D.: The ionospheric disturbance dynamo, J. Geophys. Res., 85,
605 1669–1686, https://doi.org/10.1029/JA085iA04p01669, 1980.

606 Bojilova, R., Mukhtarov, P., and Pancheva, D.: Global ionospheric response during extreme
607 geomagnetic storm in May 2024, Remote Sens., 16, 4046, https://doi.org/10.3390/rs16214046,
608 2024.

609 Cherniak, I. and Zakharenkova, I.: Evaluation of the IRI-2016 and NeQuick electron content
610 specification by COSMIC GPS radio occultation, ground-based GPS and Jason-2 joint
611 altimeter/GPS observations, Adv. Space Res., 63, 1845–1859,
612 https://doi.org/10.1016/j.asr.2018.10.036, 2019.

613 Cherniak, I. and Zakharenkova, I.: Development of the storm-induced ionospheric irregularities
614 at equatorial and middle latitudes during the 25–26 August 2018 geomagnetic storm, Space
615 Weather, 20, e2021SW002891, https://doi.org/10.1029/2021SW002891, 2022.

616 Chou, M., Yue, J., Wang, J., Huba, J. D., El Alaoui, M., Kuznetsova, M. M., Rastätter, L., Shim,
617 J. S., Fang, T., Meng, X., Fuller-Rowell, D., and Retterer, J. M.: Validation of ionospheric
618 modeled TEC in the equatorial ionosphere during the 2013 March and 2021 November
619 geomagnetic storms, Space Weather, 21, e2023SW003480,
620 https://doi.org/10.1029/2023SW003480, 2023.

621 Cnossen, I. and Förster, M.: North-south asymmetries in the polar thermosphere-ionosphere
622 system: Solar cycle and seasonal influences, J. Geophys. Res. Space Phys., 121, 612–627,
623 https://doi.org/10.1002/2015JA021750, 2016.

624 Cover, T. M. and Thomas, J. A.: Elements of Information Theory, 1st ed., Wiley, New York,
625 https://doi.org/10.1002/047174882X, 2005.

626 Dmitriev, A. V., Suvorova, A. V., Klimenko, M. V., Klimenko, V. V., Ratovsky, K. G.,
627 Rakhmatulin, R. A., and Parkhomov, V. A.: Predictable and unpredictable ionospheric

https://doi.org/10.5194/egusphere-2025-4594
Preprint. Discussion started: 2 October 2025

disturbances during St. Patrick's Day magnetic storms of 2013 and 2015 and on 8–9 March 2008, J. Geophys. Res. Space Phys., 122, 2398–2423, https://doi.org/10.1002/2016JA023260, 2017.

Endeshaw, L.: Testing and validating IRI-2016 model over Ethiopian ionosphere, Astrophys. Space Sci., 365, 49, https://doi.org/10.1007/s10509-020-03761-1, 2020.

European GNSS Service Centre (GSC): Ionospheric correction algorithm for Galileo single-frequency users (NeQuick-G), European Commission, Brussels, Belgium, 2015.

Ionospheric correction algorithms (NeQuick-G / NTCM-G): https://www.gsc-europa.eu/support-to-developers/ionospheric-correction-algorithms, last access: 2 September 2025.

Fejer, B. G.: Low latitude storm-time ionospheric electrodynamics, J. Atmos. Sol.-Terr. Phys., 64, 1401–1408, https://doi.org/10.1016/S1364-6826(02)00103-7, 2002.

Förster, M. and Cnossen, I.: Upper atmosphere differences between northern and southern high latitudes: The role of magnetic field asymmetry, J. Geophys. Res. Space Phys., 118, 5951–5966, https://doi.org/10.1002/jgra.50554, 2013.

Förster, M. and Haaland, S.: Interhemispheric differences in ionospheric convection: Cluster EDI observations revisited, J. Geophys. Res. Space Phys., 120, 5805–5823, https://doi.org/10.1002/2014JA020774, 2015.

Freedman, D. and Diaconis, P.: On the histogram as a density estimator: L2 theory, Z. Wahrscheinlichkeitstheorie verw. Geb., 57, 453–476, https://doi.org/10.1007/BF01025868, 1981.

Gonzalez, W. D., Joselyn, J. A., Kamide, Y., Kroehl, H. W., Rostoker, G., Tsurutani, B. T., and Vasyliunas, V. M.: What is a geomagnetic storm?, J. Geophys. Res. Space Phys., 99, 5771–5792, https://doi.org/10.1029/93JA02867, 1994.

Gonzalez, W. D., Echer, E., Tsurutani, B. T., Clúa de Gonzalez, A. L., and Dal Lago, A.: Interplanetary origin of intense, superintense and extreme geomagnetic storms, Space Sci. Rev., 158, 69–89, https://doi.org/10.1007/s11214-010-9715-2, 2011.

Gulyaeva, T. L., Arikan, F., and Stanislawska, I.: Inter-hemispheric imaging of the ionosphere with the upgraded IRI-Plas model during the space weather storms, Earth Planets Space, 63, 929–939, https://doi.org/10.5047/eps.2011.04.007, 2011.

Habarulema, J. B., Katamzi-Joseph, Z. T., Burešová, D., Nndanganeni, R., Matamba, T., Tshisaphungo, M., Buchert, S., Kosch, M., Lotz, S., Cilliers, P., and Mahrous, A.: Ionospheric response at conjugate locations during the 7–8 September 2017 geomagnetic storm over the Europe-African longitude sector, J. Geophys. Res. Space Phys., 125, e2020JA028307, https://doi.org/10.1029/2020JA028307, 2020.

Hernández-Pajares, M., Juan, J. M., Sanz, J., Orus, R., Garcia-Rigo, A., Feltens, J., Komjathy, A., Schaer, S. C., and Krankowski, A.: The IGS VTEC maps: A reliable source of ionospheric information since 1998, J. Geod., 83, 263–275, https://doi.org/10.1007/s00190-008-0266-1, 2009.

https://doi.org/10.5194/egusphere-2025-4594
Preprint. Discussion started: 2 October 2025

Jiang, Z., Zhang, Z., He, X., Li, Y., and Yuan, H.: Efficient and accurate TEC modeling and prediction approach with random forest and Bi-LSTM for large-scale region, Adv. Space Res., 73, 650–662, https://doi.org/10.1016/j.asr.2023.09.003, 2024.

Karatay, S., Arikan, F., and Arikan, O.: Investigation of total electron content variability due to seismic and geomagnetic disturbances in the ionosphere, Radio Sci., 45, https://doi.org/10.1029/2009RS004313, 2010.

Kashcheyev, A. and Nava, B.: Validation of NeQuick 2 model topside ionosphere and plasmasphere electron content using COSMIC POD TEC, J. Geophys. Res. Space Phys., 124, 9525–9536, https://doi.org/10.1029/2019JA026971, 2019.

Kullback, S. and Leibler, R. A.: On information and sufficiency, Ann. Math. Stat., 22, 79–86, https://doi.org/10.1214/aoms/1177729694, 1951.

Laundal, K. M. and Richmond, A. D.: Magnetic coordinate systems, Space Sci. Rev., 206, 27–59, https://doi.org/10.1007/s11214-016-0275-y, 2017.

Laundal, K. M., Cnossen, I., Milan, S. E., Haaland, S. E., Coxon, J., Pedatella, N. M., Förster, M., and Reistad, J. P.: North–south asymmetries in Earth's magnetic field: Effects on high-latitude geospace, Space Sci. Rev., 206, 225–257, https://doi.org/10.1007/s11214-016-0273-0, 2017.

Lee, W., Liu, G., Wu, D. L., and Rowland, D. E.: Ionospheric response to the 10 May 2024 geomagnetic storm as observed in GNSS radio occultation electron density, J. Geophys. Res. Space Phys., 130, e2024JA033489, https://doi.org/10.1029/2024JA033489, 2025.

Li, W., Jiang, Y., Ji, H., and Wei, W.: Amplitude scintillation detection with geodetic GNSS receivers leveraging machine learning decision tree, Satell. Navig., 5, 18, https://doi.org/10.1186/s43020-024-00136-7, 2024.

Luo, H., Gong, Y., Chen, S., Yu, C., Yang, G., Yu, F., Hu, Z., and Tian, X.: Prediction of global ionospheric total electron content (TEC) based on SAM-ConvLSTM model, Space Weather, 21, e2023SW003707, https://doi.org/10.1029/2023SW003707, 2023.

Manimegalai, M. and Bhagyaveni, M. A.: A method to enhance the throughput of cognitive radio network using Kullback-Leibler divergence with optimized sensing time (KLDOST), Wirel. Pers. Commun., 109, 1645–1660, https://doi.org/10.1007/s11277-019-06643-0, 2019.

Martinon, A. R. F., Stephany, S., and De Paula, E. R.: A new approach for the generation of real-time GNSS low-latitude ionospheric scintillation maps, J. Space Weather Space Clim., 13, 18, https://doi.org/10.1051/swsc/2023015, 2023.

Mendillo, M.: Storms in the ionosphere: Patterns and processes for total electron content, Rev. Geophys., 44, 2005RG000193, https://doi.org/10.1029/2005RG000193, 2006.

Montenbruck, O. and González Rodríguez, B.: NeQuick-G performance assessment for space applications, GPS Solut., 24, 13, https://doi.org/10.1007/s10291-019-0931-2, 2020.

Nava, B., Coïsson, P., and Radicella, S. M.: A new version of the NeQuick ionosphere electron density model, J. Atmos. Sol.-Terr. Phys., 70, 1856–1862, https://doi.org/10.1016/j.jastp.2008.01.015, 2008.

https://doi.org/10.5194/egusphere-2025-4594
Preprint. Discussion started: 2 October 2025

706 Paul, K. S., Haralambous, H., Moses, M., and Tripathi, S. C.: Effects of the October 2024 storm
707 over the global ionosphere, Remote Sens., 17, 2329, https://doi.org/10.3390/rs17132329, 2025.

708 Peng, J., Yuan, Y., Liu, Y., Zhang, H., Zhang, T., Wang, Y., and Dai, Z.: Evaluation of GNSS-
709 TEC data-driven IRI-2016 model for electron density, Atmosphere, 15, 958,
710 https://doi.org/10.3390/atmos15080958, 2024.

711 Pezzopane, M. and Pignalberi, A.: The ESA Swarm mission to help ionospheric modeling: A
712 new NeQuick topside formulation for mid-latitude regions, Sci. Rep., 9, 12253,
713 https://doi.org/10.1038/s41598-019-48440-6, 2019.

714 Pezzopane, M., Pignalberi, A., and Nava, B.: On the low-latitude NeQuick topside ionosphere
715 mismodelling: The role of parameters H0, g, and r, Adv. Space Res., 72, 1224–1236,
716 https://doi.org/10.1016/j.asr.2023.04.014, 2023.

717 Piersanti, M., De Michelis, P., Del Moro, D., Tozzi, R., Pezzopane, M., Consolini, G.,
718 Marcucci, M. F., Laurenza, M., Di Matteo, S., Pignalberi, A., Quattrociocchi, V., and Diego,
719 P.: From the Sun to Earth: Effects of the 25 August 2018 geomagnetic storm, Ann. Geophys.,
720 38, 703–724, https://doi.org/10.5194/angeo-38-703-2020, 2020.

721 Sason, I. and Verdú, S.: f-divergence inequalities, IEEE Trans. Inf. Theory, 62, 5973–6006,
722 https://doi.org/10.1109/TIT.2016.2603151, 2016.

723 Sezen, U., Arikan, F., Arikan, O., Ugurlu, O., and Sadeghimorad, A.: Online, automatic, near-
724 real time estimation of GPS-TEC: IONOLAB-TEC, Space Weather, 11, 297–305,
725 https://doi.org/10.1002/swe.20054, 2013.

726 Sherif, A., Rabah, M., Mousa, A. E., Zaki, A., and Sedeek, A.: Assessing the performance of
727 IRI-2016 and IRI-2020 models using COSMIC-2 GNSS radio occultation TEC data under
728 different magnetic activities over Egypt, J. Appl. Geod., 18, 163–176,
729 https://doi.org/10.1515/jag-2023-0068, 2024.

730 Tang, R., Zeng, F., Chen, Z., Wang, J.-S., Huang, C.-M., and Wu, Z.: The comparison of
731 predicting storm-time ionospheric TEC by three methods: ARIMA, LSTM, and Seq2Seq,
732 Atmosphere, 11, 316, https://doi.org/10.3390/atmos11040316, 2020.

733 Tsurutani, B. T., Verkhoglyadova, O. P., Mannucci, A. J., Saito, A., Araki, T., Yumoto, K.,
734 Tsuda, T., Abdu, M. A., Sobral, J. H. A., Gonzalez, W. D., McCreadie, H., Lakhina, G. S., and
735 Vasyliūnas, V. M.: Prompt penetration electric fields (PPEFs) and their ionospheric effects
736 during the great magnetic storm of 30–31 October 2003, J. Geophys. Res. Space Phys., 113,
737 2007JA012879, https://doi.org/10.1029/2007JA012879, 2008.

738 Valdés-Abreu, J. C., Díaz, M. A., Báez, J. C., and Stable-Sánchez, Y.: Effects of the 12 May
739 2021 geomagnetic storm on georeferencing precision, Remote Sens., 14, 38,
740 https://doi.org/10.3390/rs14010038, 2021.

741 Vankadara, R. K., Panda, S. K., Amory-Mazaudier, C., Fleury, R., Devanaboyina, V. R., Pant,
742 T. K., Jamjareegulgarn, P., Haq, M. A., Okoh, D., and Seemala, G. K.: Signatures of equatorial
743 plasma bubbles and ionospheric scintillations from magnetometer and GNSS observations in
744 the Indian longitudes during the space weather events of early September 2017, Remote Sens.,
745 14, 652, https://doi.org/10.3390/rs14030652, 2022.

https://doi.org/10.5194/egusphere-2025-4594
Preprint. Discussion started: 2 October 2025

746 Venugopal, I., Thampi, S. V., and Bhaskar, A.: Electrodynamic forcing of the duskside
747 ionosphere and the super fountain effect during the superstorm of 10–11 May 2024, Sci. Rep.,
748 15, 26551, https://doi.org/10.1038/s41598-025-08843-0, 2025.

749 Wang, Z., Zou, S., Liu, L., Ren, J., and Aa, E.: Hemispheric asymmetries in the mid-latitude
750 ionosphere during the 7–8 September 2017 storm: Multi-instrument observations, J. Geophys.
751 Res. Space Phys., 126, e2020JA028829, https://doi.org/10.1029/2020JA028829, 2021.

752 Xue, D., Wu, L., Xu, T., Wu, C., Wang, Z., and He, Z.: Space-weather effects on transportation
753 systems: A review of current understanding and future outlook, Space Weather, 22,
754 e2024SW004055, https://doi.org/10.1029/2024SW004055, 2024.

755 Yang, Z., Morton, Y. T. J., Zakharenkova, I., Cherniak, I., Song, S., and Li, W.: Global view
756 of ionospheric disturbance impacts on kinematic GPS positioning solutions during the 2015 St.
757 Patrick's Day storm, J. Geophys. Res. Space Phys., 125,
758 https://doi.org/10.1029/2019JA027681, 2020.

759 Zhai, C., Chen, Y., Cheng, X., and Yin, X.: Spatiotemporal evolution and drivers of the four
760 ionospheric storms over the American sector during the August 2018 geomagnetic storm,
761 Atmosphere, 14, 335, https://doi.org/10.3390/atmos14020335, 2023.

762 Zhang, S., Erickson, P. J., Vierinen, J., Aa, E., Rideout, W., Coster, A. J., and Goncharenko, L.
763 P.: Conjugate ionospheric perturbation during the 2017 solar eclipse, J. Geophys. Res. Space
764 Phys., 126, e2020JA028531, https://doi.org/10.1029/2020JA028531, 2021.

765